ACS APPLIED MATERIALS & INTERFACES

Forum Article

www.acsami.org

Influence of Poly(ethylene glycol) Segment Length on CO_2 Permeation and Stability of PolyActive Membranes and Their Nanocomposites with PEG POSS

Md. Mushfequr Rahman,[†] Volkan Filiz,*[,†] Sergey Shishatskiy,[†] Clarissa Abetz,[†] Prokopios Georgopanos,[†] Muntazim Munir Khan,[†] Silvio Neumann,[†] and Volker Abetz*[,†,‡]

[†]Helmholtz-Zentrum Geesthacht, Institute of Polymer Research, Max-Planck-Straße 1, 21502 Geesthacht, Germany

[‡]Institute of Physical Chemistry, University of Hamburg, Grindelallee 117, 20146 Hamburg, Germany

Supporting Information

ABSTRACT: Three grades of PolyActive block copolymers are investigated for CO_2 separation from light gases. The polymers are composed of 23 wt % poly(butylene terephthalate) (PBT) and 77 wt % poly(ethylene glycol terephthalate) (PEGT) having the poly(ethylene glycol) segments of 1500, 3000, and 4000 g/mol, respectively. A commercial PEG POSS (poly(ethylene glycol) functionalized polyoctahedral oligomeric silsesquioxanes) is used as a nanofiller for these polymers to prepare nanocomposites via a solvent casting method. Single gas permeabilities of N_2, H_2, CH_4, and CO_2 are measured via the time-lag method in the temperature range from 30 to 70 °C. The thermal transitions of the prepared membranes are studied by differential scanning calorimetry (DSC). It is found that the length of PEG segment has a pronounced influence on the thermal transition of the polymers that regulates the gas separation performance of the membranes. The stability of the nanocomposites is also correlated with the thermal transition of the polyether blocks of the polymer matrices.

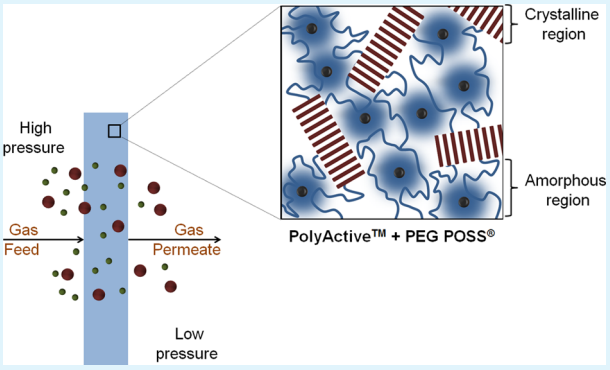

KEYWORDS: *PolyActive, PEG POSS, gas separation membrane, nanocomposite, mixed-matrix membrane*

1. INTRODUCTION

Fast and selective transport of the gas molecules through polymers has brought the membrane separation technology to the advent of a new era, leading eventually to the wide use of an energy saving and environmentally friendly gas separation process. Polymeric membranes have so far been the most attractive choice in at least 90% of the installed membrane based gas separation plants. At present, only a very few polymer materials are used to fabricate industrial membranes, although several hundreds of polymers have been reported for their gas separation properties.[1] From an application point of view the most basic requirements of a membrane material is to have a high gas permeation rate maintaining the desired selectivity. An increase of permeance reduces the membrane area required for a desired separation which results in reduced footprint and investment costs. Nonetheless, the material selection criterion also involves durability (e.g., mechanical integrity) at the operating conditions. A balance between these features to maintain high separation efficiency makes the task of material selection quite difficult. Therefore, the search for robust materials with better separation performance at the operating conditions is still going on.[2−6] This endeavor led the researchers to thoroughly examine the chemical and physical properties of the polymers which are essential to separate a particular gas mixture. In recent years, the quest has proceeded from the qualitative analysis of data to the development of quantitative models with predictive abilities facilitating directed search for advanced membrane materials.[7]

CO_2 removal occupies the central position among all the current gas separation membrane applications because of the increasing emphasis on global warming mitigation. At present fossil fuel accounts for 80% of the global energy needs which causes enormous amount of CO_2 emission. In spite of the tremendous development of alternative energy production technologies (e.g., solar energy, wind power, biomass energy, etc.) the ever growing energy requirement is expected to depend on fossil fuels at least for the next few decades.[8,9] Among the three major fossil fuel (i.e., coal, gas, and oil) coal constituents about 65% of the fossil fuel reserve and is expected to be the only remaining fossil fuel after 2042.[8] Due to the availability and low cost a large percentage of electricity

Special Issue: Forum on Polymeric Nanostructures: Recent Advances toward Applications

Received: June 29, 2014
Accepted: September 17, 2014
Published: September 30, 2014

   dx.doi.org/10.1021/am504223f | *ACS Appl. Mater. Interfaces* 2015, 7, 12289−12298

production will certainly be depended upon combustion of coal.[10] Therefore, CO_2 capture from these power plants is one of the key issues to ensure sustainability of the utilization of fossil fuel resource. Post combustion carbon capture is in principle the most appropriate technology for this purpose as it offers retrofitting the existing power plants with some modifications. In this process CO_2 is separated from the flue gas after combustion of fossil fuel, followed by transportation and storage. The major obstacle in the separation step is a wet mixture of CO_2 and N_2 having low pressure (i.e., low driving force for separation) has to be separated at a temperature range of 50−60 °C.[10,11] A vast array of potential materials has been explored to fulfill the desired requirements concerning CO_2/N_2 separation efficiency for the postcombustion carbon capture.[10] Polymers containing the polar ethylene oxide groups have a strong affinity for CO_2 due to dipole−quadrupole interaction.[12] Thus, the poly(ethylene oxide) (PEO) can be used to prepare a CO_2 selective membrane through which CO_2 passes faster than the light gases such as H_2, CH_4, N_2, etc. The major perquisite for fabrication of this class of membrane is that the PEO must be in an amorphous state at the temperature of application. A polar ether group usually increases the chain packing efficiency, but the densely packed crystallites of the polyether are impermeable and nonsorbing. For this reason the homopolymers of ethylene oxide are not suitable for membrane fabrication. Block copolymers containing alternating series of an amorphous PEO block and a rigid or even crystalline block such as polyamide, polyester, polystyrene, polyimide, etc. are suitable alternative materials.[12−14] Two commercial block copolymer families namely PolyActive[15,16] and PEBAX[17] have already proven to be suitable CO_2 selective membrane materials. These block copolymers have microphase separated structures where the crystalline block hinders the crystallization of PEO block and provides mechanical strength, whereas gas transport effectively occurs through the amorphous PEO block. A variety of different concepts have also been successfully implemented to further improve the separation performance of these commercial polymers e.g. cross-linking, incorporation of filler etc.[18,19] A fundamental approach to improve the CO_2 separation performance is to increase the total amorphous PEO content in the membrane. In this regard, several works have also been reported upon successful blend of the low-molecular-weight polyethylene glycol with these commercial block copolymers, which leads to an increase in gas permeability.[15,20−23]

In a previous work, we have used the commercial PEG POSS (poly(ethylene glycol) functionalized polyoctahedral oligomeric silsesquioxanes) as filler for two grades of the commercial multiblock copolymer family PEBAX namely PEBAX MH 1657 and PEBAX 2533. It was proved that the PEG POSS is suitable nanofiller for PEBAX MH 1657 which contains alternating series of polyethylene glycol and polyamide-6 segments.[24,25] We have also reported that the tailor-made PEG-functionalized POSS nanoparticle containing additional functionality improves the CO_2 separation performance of PEBAX MH 1657.[26,27] However, the degrees of polymerization of the polyether blocks of PEBAX multiblock copolymers are not available from the manufacturer. Therefore, in this work we incorporate PEG POSS in another polyether based block copolymer family, which is PolyActive. This multiblock copolymer family consists of poly(ethylene glycol terephthalate) soft segments and poly(butylene terephthalate) hard segments. Three grades of PolyActive are chosen for the study having poly(ethylene glycol) (PEG) segments of 1500, 3000, and 4000 g/mol, respectively. We report the CO_2 gas separation performance of these three grades of commercial polymers and their nanocomposites with PEG POSS in the temperature range from 30 to 70 °C. The aim of this work is to demonstrate how the length of poly(ethylene glycol) segment influences the separation performance and the stability of the three grades of Polyactive and the nanocomposites based on them in the temperature range of postcombustion carbon capture. In this regard, the gas transport properties are correlated with the thermoanalytical and morphological characteristics of the membranes.

2. MATERIALS AND METHODS

2.1. Materials. PolyActive 1500PEGT77PBT23, PolyActive 3000PEGT77PBT23 and PolyActive 4000PEGT77PBT23 were purchased from PolyVation, Netherlands. PEG POSS was purchased from Hybrid Plastics, USA. Chloroform (purity 99.0−99.4%) was purchased from Merck, Germany. All chemicals were used as received without any further purification.

2.2. Membrane Preparation. Polyactive membranes and their nanocomposites with PEG POSS were prepared by solution casting. Three wt percent solutions of pure polymer and the mixtures with PEG POSS were prepared using chloroform as solvent. The obtained homogeneous solutions were filtered, poured in Teflon molds and kept at room temperature for film formation. The molds were covered with a glass Petri dish to ensure slow evaporation of solvent. The PEG POSS content was varied in the range between 10 and 30 wt % with respect to the total weight of the nanocomposite. The thickness of the membranes was measured by a digital micrometer.

2.3. Characterization. The prepared membranes were characterized via constant volume, variable pressure ("time lag") method within the temperature range 30 to 70 °C. Single gas permeability, diffusion and solubility coefficients of N_2, O_2, CH_4, H_2, and CO_2 were determined. The feed pressure was 1 bar for all the gases. Each measurement was repeated 3 times and for each polymer-POSS composition, 3 membrane samples of the same composition were measured. Permeability (P), diffusion coefficient (D) and solubility (S) are determined in the temperature range of 30−70 °C from the pressure increase curves obtained during the "time-lag" experiments using the following equations

$$P = DS = \frac{V_p l}{ART\Delta t} \ln \frac{p_f - p_{p1}}{p_f - p_{p2}} \quad (1)$$

$$D = \frac{l^2}{6\theta} \quad (2)$$

where V_p is the permeate volume, l is the membrane thickness, A is the membrane area, R is the gas constant, p_f is the feed pressure considered constant in the time range Δt, p_{p1} and p_{p2} are permeate pressures at times 1 and 2, Δt is the time difference between two points (1 and 2) on the pressure curve, and θ is the time lag.

The ideal selectivity of the membranes is determined according to the following equation

$$\alpha_{A/B} = \frac{P_A}{P_B} \quad (3)$$

where, $\alpha_{A/B}$ is the ideal selectivity, and P_A and P_B are single gas permeabilities of the two gases A and B, respectively.[24,27,28]

The ^{1}H NMR spectra were recorded on an Ascend 500 (NMR magnet), AVANCE III HD spectrometer using a 90° pulse operating at a sample temperature of 298 K. From the ratios of integral areas of these peaks three rational number x_1, x_2, and x_3 are determined using the following equations

$$x_1 = \frac{I_E}{I_D} \quad (4)$$

$$x_2 = \frac{I_C + I_D}{I_A + I_B} \quad (5)$$

$$x_3 = \frac{I_C + I_D + I_E}{I_A + I_B + I_F + I_{F'}} \quad (6)$$

where I represents the integral area of a peak.

A DSC 1 (Star system) from Mettler Toledo was used to study the thermal transitions of prepared membranes in the temperature range of −100 to 250 °C using nitrogen as a purge gas stream (60 mL/min). At first the samples were heated up to 100 °C, kept there for 5 min to erase any effects resulting from sample preparation. Then they were cooled down to −100 °C and second heating scans up to 250 °C cooling scan down to −100 °C were performed. All DSC runs were performed at a scan rate of 10 K/min. The crystallinity X_c of the polyether block (listed in Table 3) is determined as

$$X_c = \frac{\Delta H}{\Delta H_c} \quad (7)$$

where ΔH is the is the melting enthalpy of polyether blocks obtained from the second heating scan of DSC run and ΔH_c is the theoretical value for melting enthalpy of 100% crystalline poly(ethylene oxide).[13] The ΔH_c value of 166.4 J/g suggested by Simon and Rutherford is used for calculation.[29]

Scanning electron microscopy (SEM) was carried out on a Zeiss "Merlin" microscope equipped with an energy dispersive microanalysis (EDS) system (Oxford). The surface and cross section morphologies were analyzed using secondary electrons (SE), energy selective backscattered electrons (EsB) and energy disperse X-rays. Cross sections were prepared under cryogenic conditions with a Leica Cryo-Ultramicrotome EM UCT FCS equipped with a diamond knife. The cross-section morphology was also studied with a Veeco MultiMode NanoScope IV atomic force microscope in TappingMode.

3. RESULTS

3.1. Composition of Three Grades of PolyActive. The commercial block copolymer PolyActive consists of two building blocks namely poly(ethylene glycol terephthalate) (PEGT) and poly(butylene terephthalate) (PBT). The three grades chosen for this study consist of 77 wt % PEGT and 23 wt % PBT. The molecular weight of the poly(ethylene glycol) segments in these polymers are 1500, 3000, and 4000 g/mol, respectively. Because the ratio of weight content of PEGT and PBT is same in these three polymers, they are addressed in terms of length of the PEG segment in this paper. The commercial names and the acronyms are listed in Table 1.

Table 1. Comparison of the Three Different Grades of Polyactive from ^{1}H NMR[a]

commercial name	acronym	x_1	x_2	x_3
PolyActive 1500PEGT77PBT23	P 1500	30.7	0.46	4.5
PolyActive 3000PEGT77PBT23	P 3000	69.6	0.23	5.1
PolyActive 4000PEGT77PBT23	P 4000	86.6	0.20	5.8

[a] x_1, x_2, and x_3 are determined from the ratios of the integral areas (I) of the ^{1}H NMR peaks. $x_1 = I_E/I_D$, $x_2 = I_C + I_D/I_A + I_B$, $x_3 = I_C + I_D + I_E/I_A + I_B + I_F + I_{F'}$.

The ^{1}H NMR spectra of three grades of PolyActive are illustrated in Figure 1. The peaks A and B at 4.43 and 1.97 ppm, respectively, originate from the butylene units of PBT. The peaks C and D at 4.5 and 3.85 ppm are attributed to the protons of the first repeating unit of PEG which is attached to the terephthalate unit i.e. the neighboring $-CH_2-CH_2-O-$ group of terephthalate unit. The rest of the repeating units of PEG blocks give the peak E at 3.64 ppm. The aromatic protons of the terephthalate units of PEGT and PBT blocks (peak F and F′) appear at 8.11 and 8.09 ppm, respectively.[30]

The rational number x_1, x_2, and x_3 determined using eqs 4, 5, and 6 are listed in Table 1. $x_1 + 2$ is the average number of ethylene oxide repeating units in PEG segments so the value increases in the following order P 1500 < P 3000 < P 4000. x_2 is the ratio of number of PEG segments to that of butadiene segments. The rational number x_3 is related to the PEG content of the polymer as it is the ratio between the sums of the integral areas of resonance for protons of PEG segment to that of all other protons. From Table 1, it is evident that variation of the PEG length changes the polymer composition, although the PEGT and PBT weight content is equal. The PEG content in the polymer (represented by x_3) increases with an increase in the length of the PEG segments (represented by x_1), whereas the number of PEG segments (represented by x_2) decreases.

3.2. Thermal Characterization. Figure 2a depicts the structure of PEG POSS provided by the supplier. It contains a cage structure of silsesquioxane as core and the poly(ethylene glycol) ligands attached to every Si atom of the cage. According to the structure each of the PEG ligands of PEG POSS is ca. 645 g/mol and the PEG content is ca. 92 wt %.[24] The thermal transitions of PEG POSS in the second heating and cooling scan of DSC are presented in Figure 2b. In the heating scan the melting starts at approximately −10 °C and the major melting peak has a peak temperature of −1 °C. The small shoulder prior to the major melting peak refers to some poorly ordered crystals. In the cooling run the crystallization exotherm is observed at approximately −22 °C.

The thermal transitions (second heating and cooling scans) of the three grades of PolyActive and their nanocomposites with PEG POSS are presented in the Supporting Information (Figure S1). The onset, peak, endset, enthalpy of melting, enthalpy of crystallization, and crystallinity of the polyether blocks of three grades of PolyActive are listed in Table 2. The crystallinity of the polyether block increases and the melting endotherm (onset, peak, and endset) shifts to a higher temperature as the length of polyether segment increases. A comparison of the onset temperatures suggests that the melting of the crystals start at a higher temperature when the polyether segment is longer. Figure S1a−c in the Supporting Information shows that the melting endotherm of the polyether block of the polymers appears exactly at the same temperature also for the nanocomposites with 10−30 wt % PEG POSS. A new melting endotherm is observed around 0 °C in cases of 20 and 30 wt % loaded nanocomposites. This new endothermic peak appears at the temperature for all the nanocomposites. Hence it is evident that it appears from the melting of poly(ethylene glycol) chains of the nanofiller PEG POSS.

The onset, peak, and endset of crystallization of the polyether blocks of the three grades of PolyActive while cooling down from the melt have the following order: P 4000 > P 3000 > P 1500. Hence, crystallization of the polyether block starts at a higher temperature when the polyether segment is longer. Figure S1d in the Supporting Information shows that the crystallization of polyether block occurs at slightly higher temperature in the nanocomposites of P 1500 compared to the pure polymer. This indicates a nucleating effect of the nanofiller as we also showed in a previous work where PEG POSS acted as a nucleating agent for the commercial multiblock copolymer PEBAX MH 1657.[24] However, this phenomenon is not observed in the nanocomposites of P 3000 and P 4000. For 20 and 30 wt % PEG POSS loaded nanocomposites a separate

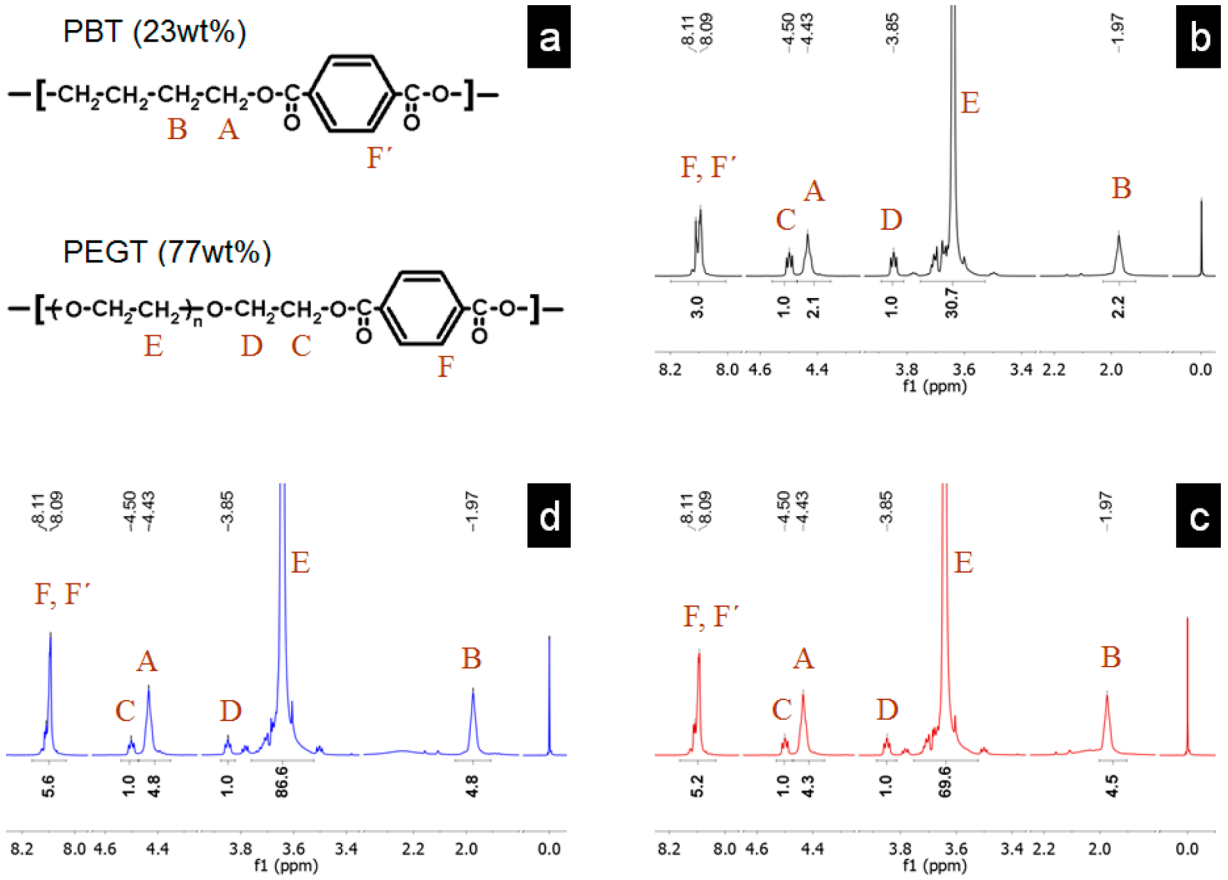

Figure 1. (a) Structure of poly(butylene terephthalate) (PBT) and poly(ethylene glycol terephthalate) (PEGT); (b) ^{1}H-NMR of P 1500; (c) ^{1}H-NMR of P 3000; (d) ^{1}H-NMR of P 4000.

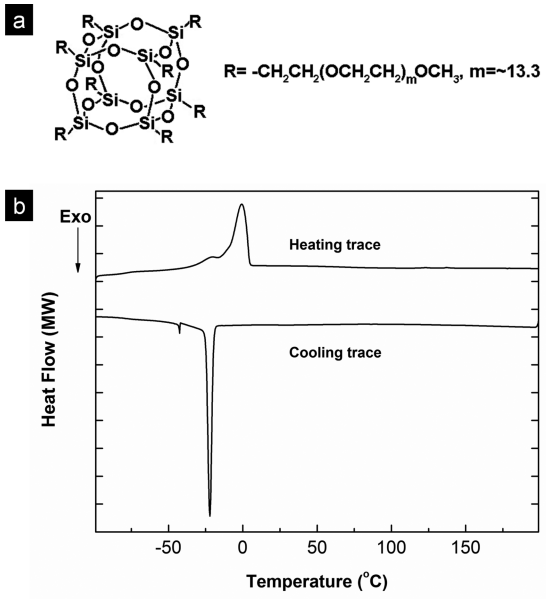

Figure 2. (a) Chemical structure and (b) DSC curves (second heating and cooling trace) of PEG POSS.

crystallization exotherm at a peak temperature of approximately −10 °C is observed. Although this peak appears at a higher temperature compared to the crystallization exotherm of pure PEG POSS (see Figure S1a in the Supporting Information), with increase in PEG POSS content it becomes bigger and the position in the temperature scale is the same for both 20 and 30 wt % PEG POSS-loaded nanocomposites. Thus, it is evident that this peak is attributed to the crystallization of PEG ligand of PEG POSS in the PolyActive matrices. Hence, the DSC study shows that variation of PEG segment length has a pronounced influence on the thermal transition (melting and crystallization) of the polyether blocks of P 1500, P 3000, and P 4000. Moreover, the PEG ligand of the nanofiller and the PEG segment of the block copolymer matrices melt and crystallize separately.

Table 2. Onset, Peak, Endset, and Enthalpy of Melting and Crystallization of the Polyether Blocks of Three Grades of PolyActive

	P 1500	P 3000	P 4000
melt onset temperature (°C)	18 ± 0.5	32 ± 0.3	40 ± 0.7
melt peak temperature (°C)	28 ± 0.9	41 ± 0.6	46 ± 1.3
melt endset temperature (°C)	32 ± 1.1	44 ± 0.7	50 ± 1.3
crystallization onset temperature (°C)	11 ± 0.2	24 ± 0.5	30 ± 0.1
crystallization peak temperature (°C)	9 ± 0.3	22 ± 0.5	28 ± 0.1
crystallization endset temperature (°C)	7 ± 0.4	18 ± 0.7	25 ± 0.4
enthalpy of melting, ΔH (J/g)	62 ± 1.4	90 ± 1.2	95 ± 1.0
enthalpy of crystallization (J/g)	61 ± 0.1	84 ± 1.6	91 ± 1.0
crystallinity, X_c (%)	37	54	57

3.3. Gas Separation Performance. *3.3.1. CO_2 Permeation.* The permeability of CO_2 through P 1500, P 3000, P 4000 and their nanocomposites with PEG POSS is plotted as a function of temperature in Figure 3. At 30 °C, P 1500 shows

dx.doi.org/10.1021/am504223f | ACS Appl. Mater. Interfaces 2015, 7, 12289−12298

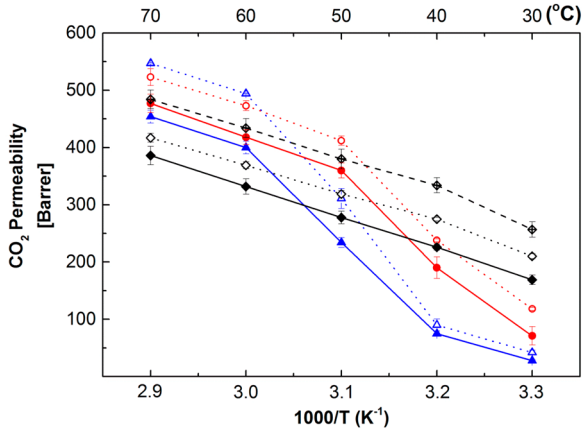

Figure 3. CO_2 permeability as a function of temperature in three grades of PolyActive and their nanocomposites with PEG POSS. Black diamonds connected by solid black line is P 1500, black diamonds connected by dotted black line is 20 wt % PEG POSS loaded P 1500 nanocomposite, black diamonds connected by dashed black line is 30 wt % PEG POSS loaded P 1500 nanocomposite, red circles connected by solid red line is P 3000, red circles connected by dotted red line is 20 wt % PEG POSS loaded P 3000 nanocomposite, blue triangles connected by solid blue line is P 4000, blue triangles connected by dotted blue line is 20 wt % PEG POSS loaded P 4000 nanocomposite.

higher permeability than P 3000 and P 4000. But between 50 and 70 °C, P 3000 has higher CO_2 permeability than the other two grades of pure polymer. It is evident that the trend of increase in gas permeability with the increase in temperature is different in the different grades of PolyActive. P 1500 shows a gradual increase of permeability with increase in temperature. For P 3000, the increase of permeability in the range of 30−50 °C is significantly high, but in the range of 50−70 °C, the trend is similar to that of P 1500. P 4000 also shows a similar behavior like P 3000 but at a higher temperature range. The nanocomposites of P 1500 with PEG POSS have higher permeabilities compared to pure P 1500. The trend of increase of permeability with the increase of temperature for both 20 and 30 wt % PEG POSS loaded nanocomposites is analogous to that of pure P 1500. The nanocomposite of P 3000 with 20 wt % PEG POSS also shows higher permeability than P 3000. In case of 20 wt % PEG POSS loaded in P 4000 the CO_2 permeability of the nanocomposite is similar to that of pure P 4000 membrane at 30 and 40 °C. But as the temperature increases, the CO_2 permeability through the nanocomposite becomes significantly higher compared to that of the P 4000 membrane. After the gas permeability measurements via time lag from 30−70 °C, the measurement cell was cooled to 30 °C again to take out the sample. It is important to mention here that a small amount of PEG POSS (confirmed by FTIR) was observed on top of the nanocomposites of P 3000 after the gas transport tests, whereas the nanocomposites of P 4000 were found broken into pieces. Because reproducible time lag curves were observed until the last gas was passed through the membrane at 70 °C, it is evident that the nanocomposites of P 4000 broke into pieces while cooling down (from 70 to 30 °C). In the case of P 1500, stable nanocomposite membranes were obtained from up to 30 wt % loading of PEG POSS. Because the nanocomposites of P 3000 and P 4000 with 20 wt % PEG POSS are not stable in the temperature range of 30−70 °C, single gas permeability measurement data of 30 wt % PEG POSS loaded nanocomposites (which are also unstable) are not mentioned in this paper. The CO_2 permeability of the P 1500, nanocomposite of P 1500 containing 30 wt % PEG POSS, P 3000 and P 4000 are listed in the Supporting Information (Table S2) together with the published result of PEBAX MH 1657 and 30 wt % PEG POSS loaded PEBAX MH 1657 nanocomposite from our previous work[24] for comparison. P 1500, P 3000, and 30 wt % PEG POSS loaded P 1500 have higher CO_2 permeabilities compared to PEBAX MH 1657 and its nanocomposite in the temperature range 50−70 °C.

Diffusion and solubility of the membranes are plotted as a function of temperature in Figures 4 and 5. It is evident from

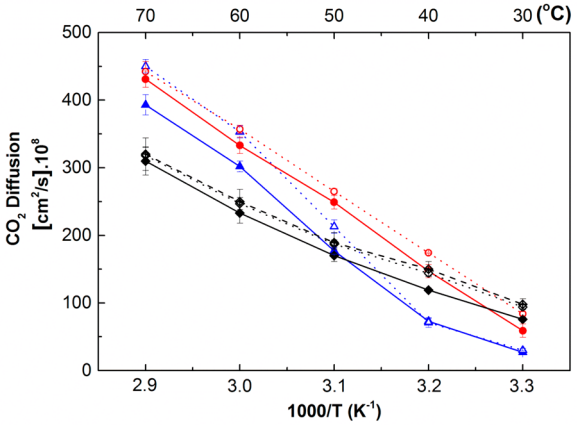

Figure 4. CO_2 diffusivity as a function of temperature in three grades of PolyActive and their nanocomposites with PEG POSS. Black diamonds connected by solid black line is P 1500, black diamonds connected by dotted black line is 20 wt % PEG POSS loaded P 1500 nanocomposite, black diamonds connected by dashed black line is 30 wt % PEG POSS loaded P 1500 nanocomposite, red circles connected by solid red line is P 3000, red circles connected by dotted red line is 20 wt % PEG POSS loaded P 3000 nanocomposite, blue triangles connected by solid blue line is P 4000, blue triangles connected by dotted blue line is 20 wt % PEG POSS loaded P 4000 nanocomposite.

Figure 4 that CO_2 has slightly higher diffusion coefficient in P 1500 than in P 3000 at 30 °C. Between 40 to 70 °C the diffusion coefficient of CO_2 is highest for P 3000 among three pure grades of polymer. The higher CO_2 diffusion coefficient with increasing temperature in P 3000 compared to P 1500 is clearly related with the length of the polyether segment. It is clear from section 3.1 that the total ether content is higher in P 3000 than in P 1500. P 4000 has the longest polyether segment and highest ether content among the three grades of pure polymer. However, the CO_2 diffusion coefficient is lower in this polymer than P 3000 within the range of 30−70 °C. At 30 and 40 °C it is even lower than that of P 1500. From the change of slope at 40 °C it is clear that the thermal transition has an influence upon the diffusion of CO_2 in this polymer (discussed later in section 4). Figure 5 shows that the different trend of increase of CO_2 permeability with the increase in temperature is largely due to the difference in CO_2 solubility. At 30 °C, CO_2 solubility in P 1500 is significantly higher compared to P 3000 and P 4000. CO_2 solubility decreases in P 1500 with the increase in temperature. In the other two pure polymers, CO_2 solubility increases up to 50 °C. At higher temperature, P 3000 shows a decreasing trend. In P 4000, a loss of solubility was observed only at 70 °C.

3.3.2. CO_2 Selectivity over Light Gases. Single gas permeability of N_2, CH_4, and H_2 are presented in the

dx.doi.org/10.1021/am504223f | ACS Appl. Mater. Interfaces 2015, 7, 12289−12298

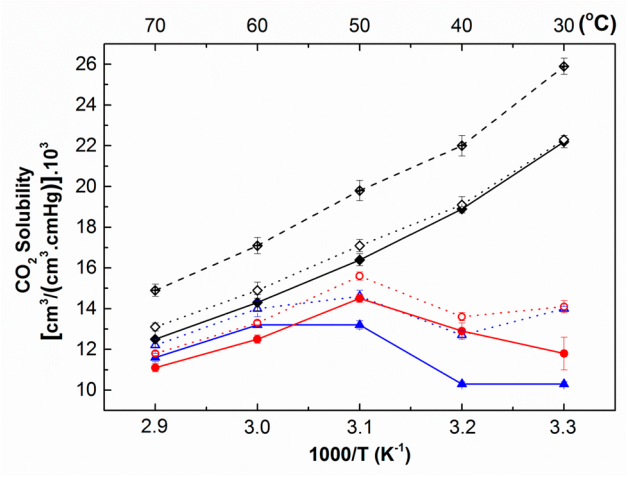

Figure 5. CO_2 solubility as a function of temperature in three grades of PolyActive and their nanocomposites with PEG POSS. Black diamonds connected by solid black line is P 1500, black diamonds connected by dotted black line is 20 wt % PEG POSS loaded P 1500 nanocomposite, black diamonds connected by dashed black line is 30 wt % PEG POSS loaded P 1500 nanocomposite, red circles connected by solid red line is P 3000, red circles connected by dotted red line is 20 wt % PEG POSS loaded P 3000 nanocomposite, blue triangles connected by solid blue line is P 4000, blue triangles connected by dotted blue line is 20 wt % PEG POSS loaded P 4000 nanocomposite.

Supporting Information (Table S1). The ideal selectivity of CO_2 over N_2, CH_4, and H_2 are calculated using eq 3. CO_2/N_2 selectivity decreases with increasing temperature for all the membranes (presented in Figure S2 in the Supporting Information). At 30 °C CO_2/N_2 selectivity of P 3000 is slightly lower than that of P 1500. Between 40 and 70 °C CO_2/N_2 selectivity of these two grades of polymer are equal. P 4000 shows lower CO_2/N_2 selectivity than other two grades of polymer up to 50 °C. PEG POSS does not alter the CO_2/N_2 selectivity of P 1500 and P 3000 nanocomposite membrane significantly. But P 4000 nanocomposite with 20 wt % PEG POSS showed better selectivity than that of pure polymer membrane. There is no significant difference in CO_2/CH_4 selectivity of three grades of pure polymer membrane (presented in Figure S3 in the Supporting Information). The nanocomposites with 20 wt % PEG POSS do not show any significant change in CO_2/CH_4 selectivity compared to the pure polymers. However, P 1500 nanocomposite with 30 wt % PEG POSS showed significantly low selectivity at 30 and 40 °C. An increase in PEG segment length leads to lower CO_2/H_2 selectivity at 30 °C (presented in Figure S4 in the Supporting Information). With the increase of temperature the CO_2/H_2 selectivity of P 1500 shows a gradual decrease. However, for P 3000 and P 4000 at 40 °C the CO_2/H_2 selectivity increases and then shows a decreasing trend with temperature. The nanocomposites of P 1500 have slightly higher CO_2/H_2 selectivity compared to the pure P 1500 membrane (presented in Figure S4 in the Supporting Information). No significant difference was observed between the P 1500 nanocomposites with 20 and 30 wt % PEG POSS. The nanocomposites of P 3000 and P 4000 with 20 wt % PEG POSS have significantly higher CO_2/H_2 selectivity at 30 °C compared to pure polymer. The trend of decreasing CO_2/H_2 selectivity with increasing temperature in these nanocomposites is different from that of P 3000 and P 4000.

3.4. Morphology. Morphology of P 1500 and its nanocomposites containing 20 and 30 wt % PEG POSS is studied using SEM and AFM. Figure 6 shows the SEM

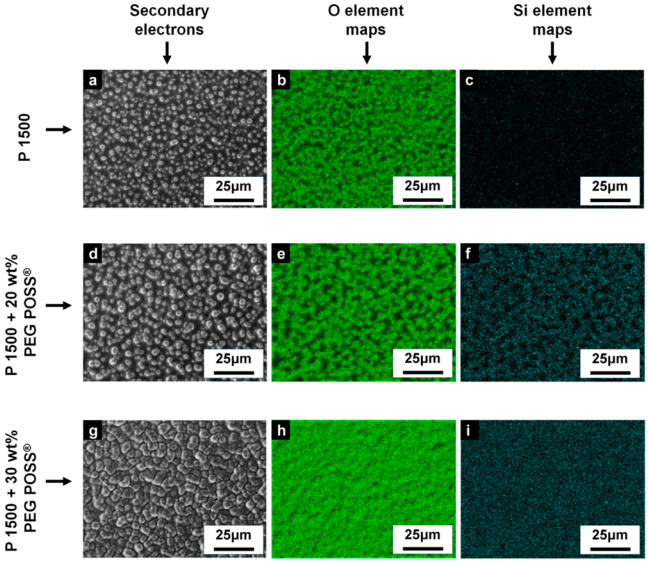

Figure 6. Surface morphology: (a) SEM micrograph of P 1500, secondary electrons (SE); (b) oxygen elemental map of P1500; (c) silicon elemental map of P 1500; (d) SEM micrograph of P 1500 + 20 wt % PEG POSS; (e) oxygen elemental map of P 1500 + 20 wt % PEG POSS; (f) silicon elemental map of P 1500 + 20 wt % PEG POSS; (g) SEM micrograph of P 1500 + 30 wt % PEG POSS; (h) oxygen elemental map of P 1500 + 30 wt % PEG POSS; (i) silicon elemental map of P 1500 + 30 wt % PEG POSS. Green dots in b, e, and h denote oxygen, whereas blue dots in c, f, and i denote silicon. The accelerating voltage is 5 kV for all measurements.

micrographs and oxygen and silicon elemental maps of the surface of P 1500 and the nanocomposite membranes taken at an accelerating voltage of 5 kV. P 1500 has spherical regions rich in oxygen (Figure 6a, b) that are attributed to the polyether blocks of the multiblock copolymer. Similar morphological features are observed in the nanocomposite membrane containing 20 wt % PEG POSS, although the size of these oxygen rich regions increases (Figure 6d, e). The Silicon elemental map (Figure 6f) reveals that the PEG POSS preferentially resides within these oxygen rich regions. Upon further increase in PEG POSS, i.e., in the nanocomposite membrane containing 30 wt % nanofiller, the oxygen-rich regions no longer form discrete microdomains (Figure 6h). The silicon elemental map (Figure 6i) also shows that PEG POSS is distributed all over the surface of this nanocomposite membrane.

The SEM micrographs and elemental mappings of the cross sections of these membranes are depicted in Figure 7. The SEM micrographs of Figures 7a, d, and g show that the morphological features are indiscernible at a macroscopic level on the cross section of the membranes. Moreover, the oxygen and silicon elemental mappings exhibit that PEG POSS is homogeneously distributed at this spatial resolution in both nanocomposites with 20 and 30 wt % PEG POSS, respectively. Interesting structural features are observed in the SEM micrographs of higher magnification presented in Figures 8a, 9a, and 10a. Taking advantage of an energy selective backscattered (EsB) incolumn detector at an accelerating voltage of 800 V, it was possible to distinguish the PEG POSS-

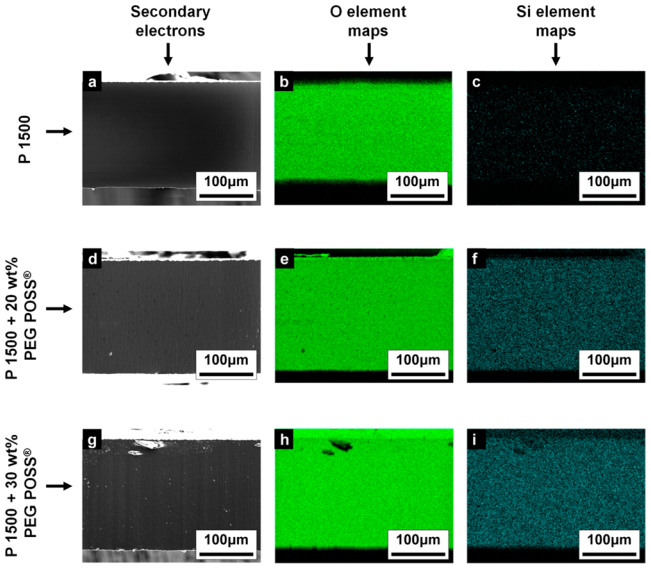

Figure 7. Cross-section morphology: (a) SEM micrograph of P 1500; (b) oxygen elemental map of P1500; (c) silicon elemental map of P 1500; (d) SEM micrograph of P 1500 + 20 wt % PEG POSS; (e) oxygen elemental map of P 1500 + 20 wt % PEG POSS; (f) silicon elemental map of P 1500 + 20 wt % PEG POSS; (g) SEM micrograph of P 1500 + 30 wt % PEG POSS; (h) oxygen elemental map of P 1500 + 30 wt % PEG POSS; (i) silicon elemental map of P 1500 + 30 wt % PEG POSS. Green dots in b, e, and h denote oxygen, whereas blue dots in c, f, and i denote silicon. The accelerating voltage is 5 kV for all measurements.

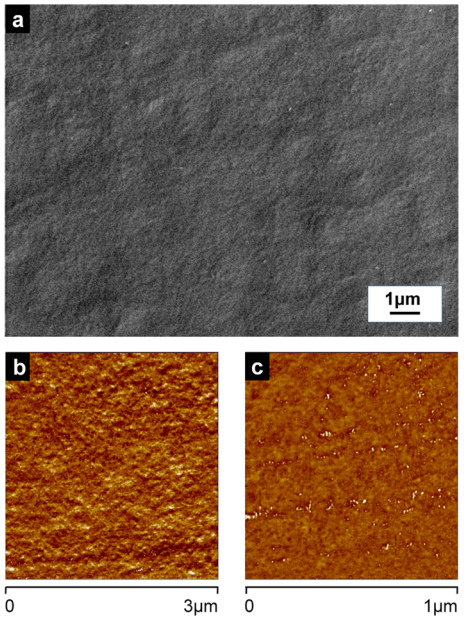

Figure 8. Cross-section of P 1500: (a) SEM image, accelerating voltage 800 V, energy selective backscattered electrons; (b) AFM image (3 × 3 μm^2); (c) AFM image (1 × 1 μm^2).

rich domains (bright colored areas) and PBT domains on a larger scale. Figure 9a shows an array of discrete elliptical domains rich in nanofiller content in the nanocomposite membrane containing 20 wt % PEG POSS. These elliptical features disappear and the PEG POSS-rich domains become interconnected when the nanofiller content is 30 wt % (Figure 10a). Because of the low magnification necessary to observe

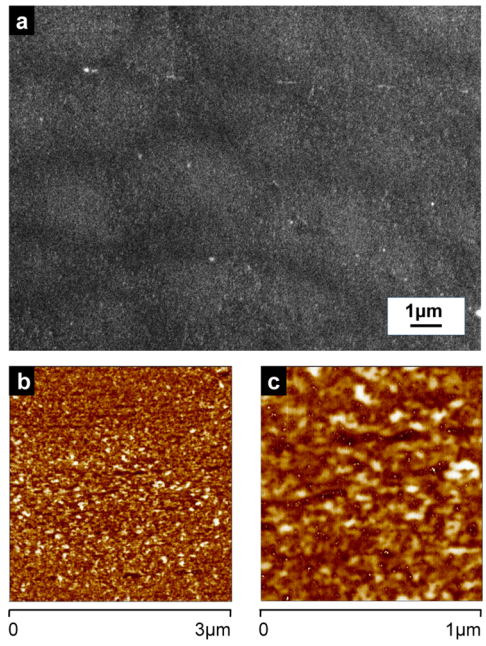

Figure 9. Cross-section of P 1500 + 20 wt % PEG POSS: (a) SEM image, accelerating voltage 800 V, energy selective backscattered electrons; (b) AFM image (3 × 3 μm^2); (c) AFM image (1 × 1 μm^2).

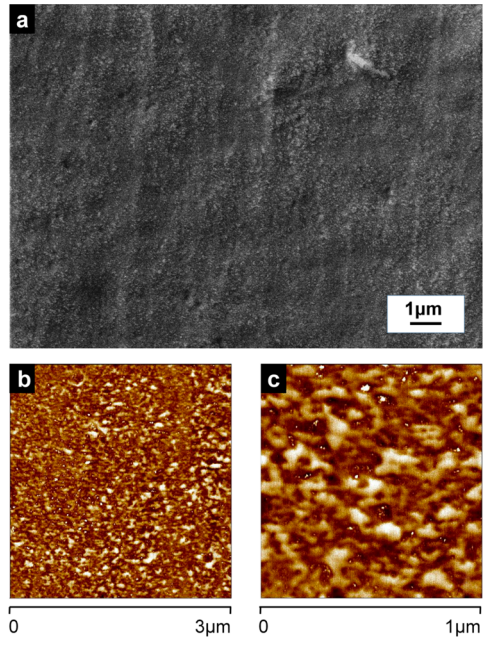

Figure 10. Cross section of P 1500 + 30 wt % PEG POSS: (a) SEM image, accelerating voltage 800 V, energy selective backscattered electrons; (b) AFM image (3 × 3 μm^2); (c) AFM image (1 × 1 μm^2).

these morphological features over a large area, the nanoscopic microphase separation of the block copolymer is not discerned in the SEM micrographs. The microphase separation of polyether and polyester domains of the P 1500 multiblock copolymer is visible in the 1 × 1 μm AFM phase image (Figure 8c). The dark brown regions correspond to the amorphous PEG domains while the light brown regions are attributed to the polyester domains. The white spots surrounded by the dark brown region are attributed to the crystallites of PEG. Appearance of these white spots suggests that the polyether

dx.doi.org/10.1021/am504223f | ACS Appl. Mater. Interfaces 2015, 7, 12289−12298

domains are not completely amorphous under the measurement condition of AFM. PEG POSS appears as white spots in TappingMode AFM phase images. The 3×3 μm^2 AFM images presented in Figures 9b and 10b show both the PEG POSS-rich regions and the regions depleted of PEG POSS in the nanocomposites. These images are in agreement with the SEM results. The microphase separated structure embedded underneath these PEG POSS depleted regions is only visible in AFM. Figures 9c and 10c show the 1×1 μm^2 AFM phase images of the regions that are rich in PEG POSS content. Both of these images show that although PEG POSS exists as agglomerates on a nanoscopic level, the nanofillers are not rejected by the polyether microdomains of both nanocomposite membranes.

4. DISCUSSION

The gas permeability increases with temperature in a polymer membrane. Typically, diffusion (i.e., the kinetic factor of permeability) increases, whereas solubility (i.e., the thermodynamic factor) shows a decreasing trend with increasing temperature.[31] In a rubbery polymer membrane, this phenomenon is attributed to higher chain mobility of the polymer membrane and higher kinetic energy of the permeating gas molecules. This trend is observed only in P 1500 among the three grades of PolyActive investigated here. Hence, it seems that the polyether blocks of P 1500 are in the amorphous state between 30 and 70 °C and no thermal transition occurs in this temperature range. In P 3000 and P 4000 another key feature dominates the transport of CO_2 through the membranes. It is apparently well-known that diffusion of gases through a semicrystalline polymer is lower than through an amorphous polymer. Crystallites of semicrystalline polymers typically act as impermeable and nonsorbing phase. Gas molecules are effectively soluble in and diffuse through only the amorphous phase. Hence the presence of crystallites increases the tortuosity of the gas diffusion path. Moreover, these crystallites cause chain immobilization of the neighboring amorphous phase to some extent.[12,32] From the CO_2 permeation behavior (section 3.3.1) it is evident that the polyether blocks of P 3000 and P 4000 are in semicrystalline state at 30 °C. With the increase of temperature the crystallites start to melt (i.e., the polymer undergoes thermal transition) and the total amount of amorphous polyether increases. P 3000 shows the typical behavior of a rubbery polymer within 50−70 °C range. Hence it seems reasonable to argue that melting of the crystallites of P 3000 is complete as the temperature increases from 30−50 °C for single gas permeation measurement. But for P 4000 the CO_2 permeation trend (Figure 3) reveals that some crystallites are still present in the polyether blocks at 50 °C. However, section 3.2 shows that according to DSC measurements at a scan rate of 10 K/min the melting of the polyether block of P 1500, P 3000, and P 4000 is completed at approximately 32, 44, and 50 °C, respectively. It must be noted that the onset and endset temperatures of the melting endotherms cannot be used directly to explain the behavior of the CO_2 permeation behavior observed at a particular temperature presented in section 3.3.1. Because the temperature recorded in DSC is a function of the scan rate and the rate of increase of temperature of the single gas permeability measurements (via time lag method) is not comparable to that of DSC scan.

Metz et al.[16] have extensively studied the poly(ethylene oxide) poly(butylene terephthalate) (PEO−PBT) multiblock copolymers and reported the CO_2 permeability of 1000PEO75PBT25, 2000PEO75PBT25, and 4000PEO75PBT25 (having polyether segments of 1000, 2000, and 4000 g/mol, respectively). It was found that 4000PEO75PBT25 at 50 °C exhibits the highest CO_2 permeability among studied polymers. A comparison of the three grades of PolyActive (containing 77 wt % PEGT and 23 wt % PBT) investigated here suggests that if the application temperature is 50 °C or slightly higher as is expected in the case of postcombustion carbon capture,[10] the P 3000 polymer would be the ideal choice among the three grades of PolyActive investigated here. However, if the application temperature is below 50 °C, the CO_2 permeability of P 3000 decreases dramatically, as the polyether blocks are not in a completely amorphous state. In this case, the nanocomposite of P 1500 containing 30 wt % PEG POSS is a better choice, because it gives the highest CO_2 permeability within 30−70 °C temperature range.

A careful comparison of the transport of CO_2 through the nanocomposites (presented in section 3.3.1) unravels some interesting phenomenon. Twenty weight percent PEG POSS loading in P 1500 and P 3000 leads to an increase in permeability. The CO_2 permeability (Figure 3) increased significantly as the PEG POSS content of the nanocomposite based on P 1500 was increased from 20 to 30 wt %. CO_2 diffusion coefficients for these two nanocomposite membranes are analogous and higher than that of pure P 1500 (Figure 4). It can mean that the polymer−filler system has reached an upper limit for the diffusive jumps of the penetrating CO_2 molecule. The increase of permeability stems from a substantial increase of CO_2 solubility (Figure 5) in the nanocomposite membrane. Surprisingly the CO_2 solubility changes significantly when PEG POSS content increases from 20 to 30 wt %, although it remains unchanged between 0 and 20 wt %. This observation implies that additional sites for CO_2 dissolution are formed only upon increasing PEG POSS content from 20 to 30 wt %. This hypothesis is consistent with the morphological features of the membranes presented in section 3.4. The microscopic investigation shows that there exists a saturation threshold of PEG POSS content between 20 and 30 wt % in P 1500, after which further incorporation of PEG POSS leads to morphological change of the nanocomposite. Isolated PEG POSS-rich regions are observed both in surface and cross section of the nanocomposite containing 20 wt % PEG POSS. In 30 wt % PEG POSS containing nanocomposite the surface has more homogeneous distribution of ether oxygen which may lead to favorable sorption of CO_2 molecules. Moreover, the PEG POSS-rich regions become continuous (i.e., not isolated anymore) in the bulk of this nanocomposite membrane. Hence, more PEG is accessible in the bulk of the nanocomposite for the penetrating CO_2 molecules due to good interconnection of PEG POSS rich regions. Thus, the morphology of the P 1500 nanocomposites has substantial influence upon the gas permeation through the membranes.

The nanocomposites of P 3000 and P 4000 are not interesting from an application point of view since they do not show stable properties under experimental conditions. From the gas transport behavior observed in section 3.3.1 for pure polymer membranes, it is clear that both P 3000 and P 4000 undergo thermal transition in the temperature range of 30−70 °C, whereas P 1500 does not. Section 3.2 demonstrates that the polyether of PEG POSS melts and crystallizes separately from the polyether of all three grades of PolyActive during heating and cooling scans of DSC run. Moreover, the

polyether of P 1500 has lower crystallinity compared to P 3000 and P 4000 (Table 2). Thus, the nanocomposite of P 1500 is stable in the temperature range of 30−70 °C because the polyether domains do not undergo any thermal transition in this temperature range. Moreover, only 37% of the polyether of P 1500 is able to crystallize. Hence, there is always enough amorphous polyether of the block copolymer present in the matrix to accommodate the PEG POSS nanofiller. These observations lead to the conclusion that the nanocomposites of PolyActive containing PEG POSS are not stable in a temperature range where the polyether blocks undergoes any thermal transition in case when crystalline phase content is big enough to force the dispersed PEG POSS out of the polymer matrix. Hence the application of PolyActive nanocomposites with PEG POSS having high crystallization degree as selective material of the gas separation membrane is only possible in a temperature range where no thermal transition takes place. Although we report this phenomenon here only for blends of PolyActive and PEG POSS, this trend will very likely be true for other PEO-based block copolymer and filler combinations as well.

5. CONCLUSION

The influence of the PEG segment length of three grades of PolyActive upon separation of CO_2 from light gases is investigated. Commercial PEG POSS is used as nanofiller to prepare the nanocomposite membranes. A correlation between the thermal transition observed in the DSC run and the gas permeation phenomenon in the temperature range from 30 to 70 °C elucidates some essential features that may facilitate the selection of appropriate membrane material for postcombustion carbon capture. The length of the PEG segment regulates the content of the crystalline polyether phase at a particular temperature, which has a pronounced influence on the gas separation efficiency of the membrane. Commercial PEG POSS as nanofiller can increase the gas permeability, but the polymer matrix must be carefully chosen depending on the lengths of the PEG segments and the temperature range of the application. The possible application of the PEG POSS containing nanocomposite membranes based on PolyActive with high crystalline phase content is limited only in a temperature range where no thermal transition of the polyether block microphase takes place.

■ ASSOCIATED CONTENT

Supporting Information

DSC curves of the three grades of PolyActive and their nanocomposites with PEG POSS (Figure S1); permeability of N_2, CH_4, and H_2 (Table S1); CO_2/N_2 selectivity (Figure S2); CO_2/CH_4 selectivity (Figure S3); CO_2/H_2 selectivity (Figure S4); comparison of CO_2 permeability of the presented membranes with previously published PEBAX MH 1657 membranes (Table S2); Robeson Plot 2008 for CO_2/N_2 gas pair (Figure S5); Robeson Plot 2008 for CO_2/CH_4 gas pair (Figure S6). This material is available free of charge via the Internet at http://pubs.acs.org/.

■ AUTHOR INFORMATION

Corresponding Authors

*E-mail: volkan.filiz@hzg.de.
*E-mail: volker.abetz@hzg.de.

Notes

The authors declare no competing financial interest.

■ ACKNOWLEDGMENTS

The authors acknowledge financial support from the Helmholtz Association of German Research Centres through the Helmholtz Portfolio MEM-BRAIN.

■ REFERENCES

(1) Baker, R. W. Future Directions of Membrane Gas Separation Technology. *Ind. Eng. Chem. Res.* **2002**, *41*, 1393−1411.
(2) Koros, W. J. Gas Separation Membranes: Needs for Combined Materials Science and Processing Approaches. *Macromol. Symp.* **2002**, *188*, 13−22.
(3) Freeman, B. D.; Pinnau, I. Polymeric Materials for Gas Separations. In *Polymer Membranes for Gas and Vapor Separation*; American Chemical Society: Washington, D.C., 1999; Chapter 1, pp 1−27.
(4) Nguyen, Q. T.; Sublet, J.; Langevin, D.; Chappey, C.; Marais, S. é. p.; Valleton, J.-M.; Epaillard, F. P.-. CO_2 Permeation with Pebax®-Based Membranes for Global Warming Reduction. In *Membrane Gas Separation*; Yampolski, Y.; Freeman, B., Eds.; John Wiley & Sons: West Sussex, U.K., 2010; Chapter 13, pp 255−258.
(5) Gupta, Y.; Hellgardt, K.; Wakeman, R. J. Enhanced Permeability of Polyaniline Based Nano-Membranes for Gas Separation. *J. Membr. Sci.* **2006**, *282*, 60−70.
(6) Bernardo, P.; Drioli, E.; Golemme, G. Membrane Gas Separation: A Review/State of the Art. *Ind. Eng. Chem. Res.* **2009**, *48*, 4638−4663.
(7) Yampolskii, Y. Polymeric Gas Separation Membranes. *Macromolecules* **2012**, *45*, 3298−3311.
(8) Shafiee, S.; Topal, E. When will Fossil Fuel Reserves be Diminished? *Energy Policy* **2009**, *37*, 181−189.
(9) Pazheri, F. R.; Othman, M. F.; Malik, N. H. A Review on Global Renewable Electricity Scenario. *Renewable Sustainable Energy Rev.* **2014**, *31*, 835−845.
(10) Merkel, T. C.; Lin, H. Q.; Wei, X. T.; Baker, R. Power Plant Post-Combustion Carbon Dioxide Capture: An Opportunity for Membranes. *J. Membr. Sci.* **2010**, *359*, 126−139.
(11) Favre, E. Membrane Processes and Postcombustion Carbon Dioxide Capture: Challenges and Prospects. *Chem. Eng. J.* **2011**, *171*, 782−793.
(12) Lin, H. Q.; Freeman, B. D. Materials Selection Guidelines for Membranes that Remove CO_2 from Gas Mixtures. *J. Mol. Struct.* **2005**, *739*, 57−74.
(13) Lin, H.; Freeman, B. D. Gas Solubility, Diffusivity and Permeability in Poly(ethylene oxide). *J. Membr. Sci.* **2004**, *239*, 105−117.
(14) Yave, W.; Szymczyk, A.; Yave, N.; Roslaniec, Z. Design, Synthesis, Characterization and Optimization of PTT-b-PEO Copolymers: A New Membrane Material for CO_2 Separation. *J. Membr. Sci.* **2010**, *362*, 407−416.
(15) Car, A.; Stropnik, C.; Yave, W.; Peinemann, K. V. Tailor-Made Polymeric Membranes based on Segmented Block Copolymers for CO_2 Separation. *Adv. Funct. Mater.* **2008**, *18*, 2815−2823.
(16) Metz, S. J.; Mulder, M. H. V.; Wessling, M. Gas-Permeation Properties of Poly(ethylene oxide) Poly(butylene terephthalate) Block Copolymers. *Macromolecules* **2004**, *37*, 4590−4597.
(17) Bondar, V. I.; Freeman, B. D.; Pinnau, I. Gas Transport Properties of Poly(ether-b-amide) Segmented Block Copolymers. *J. Polym. Sci., Part B: Polym. Phys.* **2000**, *38*, 2051−2062.
(18) Sridhar, S.; Suryamurali, R.; Smitha, B.; Aminabhavi, T. M. Development of Crosslinked Poly(ether-block-amide) Membrane for CO_2/CH_4 Separation. *Colloids Surf., A* **2007**, *297*, 267−274.
(19) Murali, R. S.; Sridhar, S.; Sankarshana, T.; Ravikumar, Y. V. L Gas Permeation Behavior of Pebax-1657 Nanocomposite Membrane Incorporated with Multiwalled Carbon Nanotubes. *Ind. Eng. Chem. Res.* **2010**, No. 49, 6530−6538.

(20) Yave, W.; Car, A.; Funari, S. S.; Nunes, S. P.; Peinemann, K.-V. CO_2-Philic Polymer Membrane with Extremely High Separation Performance. *Macromolecules* **2010**, *43*, 326−333.
(21) Car, A.; Stropnik, C.; Yave, W.; Peinemann, K. V. PEG Modified Poly(amide-b-ethylene oxide) Membranes for CO_2 Separation. *J. Membr. Sci.* **2008**, *307*, 88−95.
(22) Yave, W.; Car, A.; Peinemann, K. V. Nanostructured Membrane Material Designed for Carbon Dioxide Separation. *J. Membr. Sci.* **2010**, *350*, 124−129.
(23) Lillepärg, J.; Georgopanos, P.; Shishatskiy, S. Stability of Blended Polymeric Materials for CO_2 Separation. *J. Membr. Sci.* **2014**, *467*, 269−278.
(24) Rahman, M. M.; Filiz, V.; Shishatskiy, S.; Abetz, C.; Neumann, S.; Bolmer, S.; Khan, M. M.; Abetz, V. PEBAX® with PEG Functionalized POSS as Nanocomposite Membranes for CO_2 Separation. *J. Membr. Sci.* **2013**, *437*, 286−297.
(25) Rahman, M. M.; Filiz, V.; Shishatskiy, S.; Neumann, S.; Khan, M. M.; Abetz, V. PEG Functionalized POSS Incorporated PEBAX Nanocomposite Membranes. *Procedia Eng.* **2012**, *44*, 1523−1526.
(26) Rahman, M. M.; Filiz, V.; Khan, M. M.; Gacal, B. N.; Abetz, V., Functionalization of POSS Nanoparticles and Fabrication of Block Copolymer Nanocomposite Membranes for CO_2 Separation. *React. Funct. Polym., DOI:* 10.1016/j.reactfunctpolym.2014.07.006.
(27) Rahman, M. M.; Shishatskiy, S.; Abetz, C.; Georgopanos, P.; Neumann, S.; Khan, M. M.; Filiz, V.; Abetz, V. Influence of Temperature upon Properties of Tailor-Made PEBAX® MH 1657 Nanocomposite Membranes for Post-Combustion CO_2 Capture. *J. Membr. Sci.* **2014**, *469*, 344−354.
(28) Shishatskiy, S.; Pauls, J. R.; Nunes, S. P.; Peinemann, K. V. Quaternary Ammonium Membrane Materials for CO_2 Separation. *J. Membr. Sci.* **2010**, *359*, 44−53.
(29) Simon, F. T.; Rutherfod, J. M. Crystallization and Melting Behavior of Polyethylene Oxide Copolymers. *J. Appl. Phys.* **1964**, *35*, 82−86.
(30) Fakirov, S.; Gogeva, T. Poly(ether ester)s Based on Poly(butylene terephthalate) and Poly(ethylene glycol), 2. Effect of Polyether Segment Length. *Makromol. Chem. Phys.* **1990**, *191*, 615−624.
(31) Zimmerman, C. M.; Koros, W. J. Polypyrrolones for Membrane Gas Separations. II. Activation Energies and Heats of Sorption. *J. Polym. Sci., Part B: Polym. Phys.* **1999**, *37*, 1251−1265.
(32) Stern, S. A.; Frisch, H. L. The Selective Permeation of Gases through Polymers. *Annu. Rev. Mater. Sci.* **1981**, *11*, 523−550.